*Journal of The Electrochemical Society*, **160** (9) H604-H611 (2013)
0013-4651/2013/160(9)/H604/8/$31.00 © The Electrochemical Society

# Bis(trifluoromethylsulfonyl)imide ($NTf_2$)-Based Ionic Liquids for Facile Methane Electro-Oxidation on Pt

**Zhe Wang* and Xiangqun Zeng**,z**

*Chemistry Department, Oakland University, Rochester, Michigan 48309, USA*

Methane electro-oxidation was investigated and systematically characterized on three different electrodes (i.e. platinum, gold and carbon electrodes) with six different ionic liquids (ILs) by Cyclic Voltammetry (CV). At platinum electrode in bis(trifluoromethylsulfonyl)imide ($NTf_2$) based ionic liquids (ILs), facile methane electro-oxidation is observed suggesting a unique catalytic Pt-$NTf_2$ interface for electron transfer reaction of methane. Little methane electro-oxidation signal is observed in ILs with other anions. The final methane oxidation products in [$C_4$mpy][$NTf_2$] is confirmed to be $CO_2$ and water by in-situ infrared spectroelectrochemistry. In contrast to many reported methane catalytic oxidation systems, there is no incomplete methane oxidation products observed. The electrochemical oxidation of methane at Pt and [$C_4$mpy][$NTf_2$] interface depends on the methane concentration linearly (from 1%~10 vol.% methane concentration). The characteristic of peak potential shifts of the oxygen redox processes in the multiple cycle CV study is consistent with the electrode reaction of oxygen coupled with chemical reactions of $CO_2$ and water which further confirms the products of methane electrode oxidation are $CO_2$ and water. The cumulative results lead us to propose a mechanism suggesting a potential catalytic system of methane oxidation in $NTf_2$ based ILs that strongly depends on the properties of the ILs and the electrode materials.
 [DOI: 10.1149/2.039309jes] 

Manuscript submitted May 8, 2013; revised manuscript received June 12, 2013. Published July 10, 2013.

Methane is one of the most abundant organic compounds on earth. Significant efforts are made to understand methane oxidation mechanisms for different applications. For example, for the development of hydrocarbon fuel cell, complete anodic oxidation of methane to carbon dioxide and water at useful current densities and low over potential is desired. However, incomplete oxidation of methane to methanol is beneficial for using methane as chemical feedstock since transporting methane or even liquified natural gas is not economical.[1–5] Methane is the main constituent of natural gas and it is one of the major constituents of landfill gas and mine gas. Unmonitored methane can accumulate which poses the greatest explosion hazards. The understanding of methane chemistry is essential for the development of robust methane sensors for the occupational and industry safety. Methane is very stable and the C-H bond in methane is one of the strongest C-H bonds (104 kcal/mol).[6,7] Except for reactions with chlorine or oxygen, methane is mostly chemically inert and is odorless and colorless. The electrochemical oxidation of methane is thermodynamically favored, but kinetically it is very slow. Significant research activities in designing and characterizing of catalytic electrode reactions for methane oxidation have been reported using microscopic, spectroscopic and electrochemical techniques.[1,8,9] Among various methods, electrochemical oxidation of methane has many benefits since the application of a potential or a current at the metal catalyst/electrolyte interface allows the manipulation or modification of the activity of the electrode catalysts.[10] The most effective catalysts for the oxidation of methane are platinum and palladium–based catalysts. However, the life-times of metal catalysts are limited by the presence of incomplete oxidation products especially CO which can poison the electrodes. The electrocatalysts or electrochemical systems that allow direct oxidation of methane to complete products, $CO_2$ and $H_2O$ at relatively low temperatures (e.g., from about 60°C to 150°C) have been investigated in the last half century. However, these systems either require specific electrolyte (e.g. strong acid or alkaline),[5,11] or exhibit extremely slow electrode kinetics at room temperature (e.g. limited catalytic activity, short catalytic life or low product selectivity[12,13]) which hinder the large-scale commercial applications using methane.

Ionic liquids (ILs) are organic electrolytes containing charge-diffuse cations and anions which display negligible vapor pressure, frequently coupled with high operational (chemical, redox, thermal, radiological) stability.[14–16] This unique combination of properties motivates our laboratory and others to investigate their applications as electrolytes for electrochemical applications (e.g. batteries, sensors etc.).[17–20] So far there is no methane oxidation reported in ionic liquids. Even though methane electro-oxidation was studied in non-aqueous electrolytes, different mechanisms of methane oxidation were proposed suggesting a complex process that was likely solvent dependent. In this work, we are motivated to investigate the roles of the electrode materials as well as the cations and anions of different ILs on methane electro-oxidation process. We attempt to determine the mechanism of electro-oxidation of methane in these ILs by cyclic voltammetry and in-situ infrared spectroelectrochemistry. Not only ILs provide the opportunity for increasing the solubility of methane and allow the ease of removal of the oxidation products, we hypothesize that ILs can facilitate a unique electrode-electrolyte interface formation which could exhibit new catalytic properties for oxidizing methane. For example, ILs could provide a strong polar environment, wherein the C–H bond in methane can be activated electrostatically. This is beneficial for the abstraction of the H from $CH_4$, and further polarization of CHx makes it easier to dissociate additional C–H bonds, increasing the efficiency of methane oxidation. It is noted that $NTf_2^-$ can adsorb on the metallic oxide surface[21] and coordinated with metal to form complexes[22] which has high catalytic activity.[23–25] Our study in this work leads us to propose a mechanism suggesting a reasonable catalytic system of methane oxidation in room temperature $NTf_2$ based ILs at Pt electrode.

## Experimental

1-butyl-1-methylpyrrolidinium bis(trifluoromethylsulfonyl)imide ([$C_4$mpy][$NTf_2$]), 1-hexyl-1-methylpyrrolidinium bis(trifluoromethylsulfonyl)imide ([$C_6$mpy][$NTf_2$]), 1-butyl-3-methylimidazolium bis(trifluoromethylsulfonyl)imide ([$C_4$mim][$NTf_2$]), 1-butyl-1-methylpyrrolidinium hexafluorophosphate ([$C_4$mpy][$PF_6$]), 1-butyl-1-methylpyrrolidinium tris(pentafluoroethyl)trifluorophosphate ([$C_4$mpy][FAP]) and 1-butyl-1-methylpyrrolidinium bis(trifluoromethylsulfonyl)imide ([$C_4$mpy][Beti]) were prepared by standard literature procedures[26–28] and structures listed in Table S1. The 0.5 and 1.0-mm diameter Pt wire, and 100-mesh Pt and Au gauze were purchased from Sigma-Aldrich (St. Louis, MO). High purity (99.99%) gases (i.e., dry air, nitrogen, methane, oxygen) were obtained from Airgas Great Lakes (Independence, OH).

A back flow electrochemical gas cell was used in this study. Similar electrochemical set-up was used in our early IL oxygen sensor work.[17] Briefly, as shown in Figure 1 and Figure S1, the working electrode is a 100-mesh platinum gauze (area is 0.64 $cm^2$) that was pressed directly onto a gas-permeable porous Teflon membrane (Zitex TM, Chemplast, Incorporated, Wayne, New Jersey) with direct contact to

*Electrochemical Society Student Member.
**Electrochemical Society Active Member.
zE-mail: zeng@oakland.edu

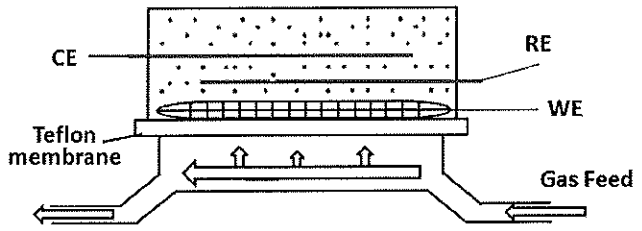


**Figure 1.** Schematic side-profile of electrochemical cell for methane oxidation in IL electrolytes. Figure abbreviations as follows: counter electrode (CE); reference electrode (RE); working electrode (WE) pressed on the Teflon membrane.

a thin layer of the IL electrolyte. This set-up minimizes the limitation of the high viscosity of ILs and allows methane to be oxidized at the gas/solid/liquid interface (tbp). Pt gauze electrode is used rather than traditional sputtered platinum or platinum black electrode[8,29] since sputtered platinum or platinum black electrode can be deactivated in the presence of oxygen. Two 0.5-mm diameter polycrystalline platinum wires were used as counter and quasi-reference electrodes. A Kel-F block (Figure 1) allows all three electrodes being arranged into a sandwich structure. The electrochemical cell was placed in a homemade dry box with temperature at 25 ± 1°C. The total gas flow was controlled at 200 sccm by digital mass-flow controllers (MKS Instruments Inc). All gas analytes (e.g. methane, air or the mixture) were prepared by pre-mixing the gases in a glass bottle with a stirring fan before introducing them into the electrochemical cell.

The electrochemical characterization was performed with a VersaStatMC Potentiostat (Princeton AMETEK US). All potentials were referenced to the platinum quasi reference electrode potential. Pt/air electrode is very often used as a pseudoreference electrode (or quasi reference electrode) in amperometric solid-state gas sensors based on solid polymer electrolytes. In our dry ionic liquid system in which the water is limited to less than 1 ppm, the Pt can be a good quasi reference electrode here.[30,31] The ferrocene/ferrocenium redox couple in the same IL was used for the calibration of the redox potential throughout this study (Figure S2).[32]

The in-situ infrared spectroelectrochemical (IR-SEC) electrodes and spectrometer configurations are illustrated in Figure 2. In specular reflection infrared spectroelectrochemistry, the sample must be reflective or on a reflective surface so that the information obtained is directly related to the thin layers at the electrode solution interface. Thus the sputtered platinum electrode on the glass or silicon provides a reflective and smooth surface which is preferred over a Pt gauze electrode. The working (8 × 8 $mm^2$) and reference (8 × 1.5 $mm^2$) electrodes were sputtered with platinum of about 200 nm layer thickness on each glass slide respectively. The counter electrode is a Pt wire. A thin layer, about 100 μm thick of the IL electrolyte was added on the electrode surfaces. A 1.5 mm height Viton barrier surrounding the cell was pressed on the glass slide to hold the IL. Before testing, the whole system was placed in the FTIR chamber and dry air or pure oxygen was purged to the system for 3 hours to remove moisture and $CO_2$ in the background. In-situ IR spectra were obtained in the reflectance mode with *p*-type polarized IR light. Polarized light can improve the signal to noise ratio over non-polarized light. Spectra of the Pt electrode without IL in the dry air or pure oxygen were collected as background spectra. The background spectra were subtracted from all other FTIR measurements (i.e. those with ILs, IL + $CH_4$, and IL+ $CH_4$ with applied potential). Varian Excalibur series 3100 FTIR spectrometer with a liquid nitrogen-cooled MCT detector was used to obtain all IR spectra.

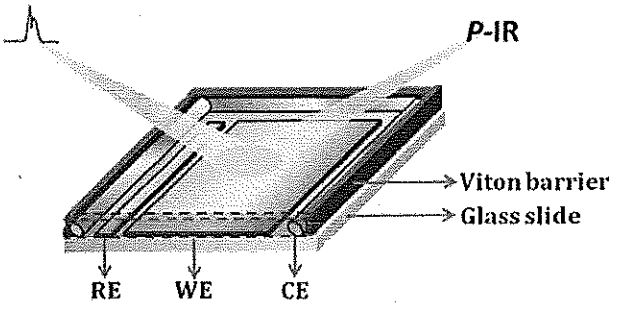


**Figure 2.** Schematic diagram of the side-view of the IR spectroelectrochemical electrodes set-up. Figure abbreviations as follows: counter electrode (CE); *p*-type polarized IR light (p-IR); reference electrode (RE); working electrode (WE).

## Results and Discussion

*Characterization of methane oxidation in different ILs by CV.*— Electrochemical oxidation of methane was typically carried out in strong acidic electrolytes because hydroxide electrolytes react with CO or $CO_2$, the products of the anodic oxidation of methane, yielding formate and carbonate. ILs provide many benefits as electrolytes for methane oxidation since it is nonvolatile and the products of oxidation of methane can be quickly solubilized in the ILs or removed from electrochemical system by gas flow. We select the low viscosity hydrophobic [$C_4$mpy][$NTf_2$], [$C_6$mpy][$NTf_2$], [$C_4$mim][$NTf_2$] and [$C_4$mpy][Beti] electrolytes. Addition experiment procedures were used to minimize the amount of water in our ionic liquid system. Before each experiment, ionic liquids were dried at ca. 100°C in vacuum for 24 hour until no visible signs of water were present in the IR spectrum ($CaF_2$ plates) following the procedures reported.[33] Using this drying process, the water level could be limited lower than 1 ppm in our ionic liquids system,[34] so that the oxidation of methane will be favored and the interference from water in these IL systems can be minimized or avoided. Figure 3 shows the CVs in these four ILs in the presence of 5% methane at Pt electrode using dry air as the dilution gas. In all these ILs, peaks of reduction of oxygen to superoxide and the subsequent oxidation of superoxide are shown at around −1.2 V and −0.7 V respectively. The oxygen redox process in ILs was well-studied, for example, Munakata et. al.[35] characterized oxygen reduction reaction in three ionic liquids (dema-FSI, dema-TFSI, dema-BETI where anion FSI is Bis(fluorosulfonyl)imide and BETI is bis(pentafluoroethanesulfonyl) imide. The cation is N,N-diethylmethuamine (dema), which is a protic cation. They found that oxygen reduction currents increased with the length of fluoroalkyl chain due to lesser of the surface adsorption of bulky anion on Pt

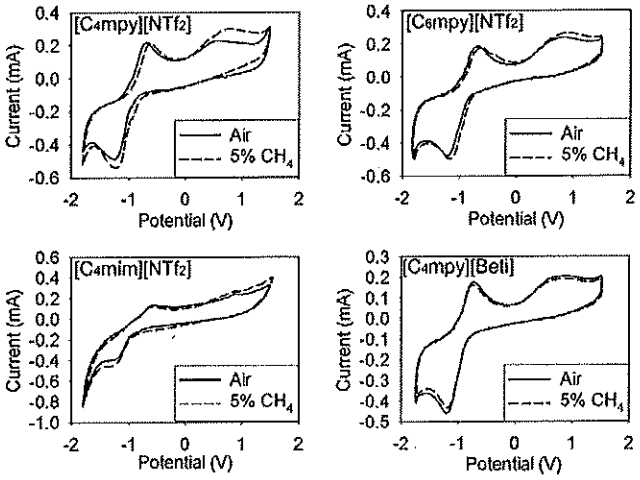


**Figure 3.** Cyclic voltammograms of Pt electrode in four ionic liquids ([$C_4$mpy][$NTf_2$], [$C_6$mpy] [$NTf_2$], [$C_4$mim][$NTf_2$] and [$C_4$mpy][Beti]) with 100% air and 5% methane in air (500 mV $s^{-1}$ scan rate, 6th cycle).

electrode than that of smaller anion. Since [$NTf_2$], [Beti] and [FAP] anions are all bulky, their adsorption on Pt is weaker in neutral ionic liquids compared with acidic media. In our system, the oxygen reduction currents in different ionic liquids were only dependent on solubility and the diffusion coefficient of $O_2$ and superoxide, (Figure 3 and Figure S3) which was related to the viscosity of ionic liquids in the following order: [$C_4$mpy][FAP] > [$C_4$mpy][Beti] > [$C_4$mpy][$NTf_2$].[36] In the absence of methane with only air in the system, the oxygen reduction is relatively more reversible with higher currents in [$C_4$mpy][$NTf_2$] electrolyte compared to that in the other ionic liquids since [$C_4$mpy][$NTf_2$] has lower viscosity and higher conductivity than that of [$C_6$mpy][$NTf_2$] and [$C_4$mpy][Beti]. A broad anodic peak is observed at ~0.7 V which was explained as Pt oxidation peak in these ILs. In contrast to [$C_4$mpy][$NTf_2$], [$C_6$mpy] [$NTf_2$], [$C_4$mpy][FAP] (Figure S3) and [$C_4$mpy][Beti], smaller peak currents were observed both in oxygen redox process and Pt oxidation process in the [$C_4$mim] [$NTf_2$] (Figure 3). It was explained that the stronger adsorption of cation $[C_4mim]^+$ on Pt surface than that of other cations resulted in the differences of double layer charging current observed in these four IL electrolytes.[37,38] As a result of the adsorption of $[C_4mim]^+$, it is more difficult for oxygen to adsorb at the electrode which hinders both Pt oxidation process and the oxygen redox process at platinum electrode. Our results are consistent with those observed by others.[17,35,39]

Comparing the CVs in the presence of 5% methane to those in pure air, only in the $NTf_2$ based ionic liquids, a broad anodic peak around 0.9 V was observed. It was rationalized that this peak is due to the oxidation of methane. The anodic peak current at +0.9 V is larger in [$C_4$mpy] [$NTf_2$] than that in [$C_6$mpy][$NTf_2$], since the [$C_6$mpy][$NTf_2$] has higher viscosity and the mass transfer is slower than that in [$C_4$mpy] [$NTf_2$]. However in [$C_4$mim] [$NTf_2$] which has the lowest viscosity among the four ILs tested, the anodic current at 0.9 V is the smallest. This observation is consistent with early rationalization that the adsorption of cation [$C_4$mim] limits the access of methane to the electrode surface subsequently prevents the methane oxidation processes. In [$C_4$mpy][Beti] electrolyte, there is no methane oxidation peak found. Although [Beti] has a similar chemical structure to the [$NTf_2$] with the same coordinated element N, the large size of [Beti] leads to a different IL-electrode interface from those $NTf_2$ based ILs because of the steric effect. The methane cannot be oxidized in [$C_4$mpy][Beti]. All above results indicate that [$NTf_2$] anion play a critical role in methane oxidation at Pt electrode.

*Characterization of the electrode-IL interface double layer property in [$C_4$mpy] [$NTf_2$].*— The CV results imply that the double layer structure of [$C_4$mpy][$NTf_2$] is unique toward methane adsorption subsequently facilitating methane oxidation. As shown in Figure S4 and S5, at 100% methane, a peak was observed in both anodic and cathodic potential scan. This peak is not observed in the presence of nitrogen so it is due to the adsorption of methane. This initial adsorption step is hypothesized to be the dissociation of a single hydrogen atom, i.e. $CH_4 \rightarrow CH_3$ (ads) + H (ads).The theoretical adsorption reaction is proposed to be $CH_4 \rightarrow CH_3$-Pt + $H^+$ + e.[40,41] The methane surface coverage could be calculated via integration of the voltammetric current signal of 100% methane in [$C_4$mpy][$NTf_2$] (Figure S4 and S5). The surface coverage of methane was calculated to be 1.16 nM/$cm^2$.

Baldalli's group has studied the CO adsorption at [$C_4$mim] [$NTf_2$]–Pt electrode interface by EIS and SFG. Recently, we report a simple method to quantify the methane adsorption at the [$C_4$mpy][$NTf_2$]–Au electrode interface by differential capacitance.[42] Our results show that the double layer of [$C_4$mpy][$NTf_2$] is highly selective to adsorb methane on the Au electrode interface. Under DC bias of −0.3 V, the double layer thickness of ionic liquid increases due to the methane adsorption resulting in a decrease of the double layer capacitance. The methane adsorption in [$C_4$mpy] [$NTf_2$] obeys Langmuir adsorption mechanism and could be quantified by measuring the change of double layer capacitance. The real part of differential capacitance at low frequency (Cre) was assigned to the double layer capacitance in the total capacitance of [$C_4$mim] [$NTf_2$]-electrode interface. In our current Pt electrode system, a Cre versus potential curve was obtained in

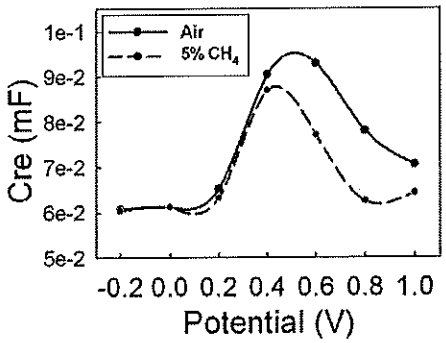


**Figure 4.** The capacitance-potential curves when the IL electrochemical system was exposed to air or 5% methane at 1 Hz. Potential scanned from −0.2 V to 1 V in [$C_4$mpy] [$NTf_2$].

[$C_4$mpy] [$NTf_2$] under air and 5% methane. As shown in Figure 4, the maximum capacitance change in the presence of 5% methane occurred at about 0.4 V. So far only in [$C_4$mpy][$NTf_2$], there is strong evidence of methane adsorption. We rationalize that the adsorption of methane at [$C_4$mpy] [$NTf_2$]-Pt or Au electrode interface is the main reason for the highest current of methane oxidation shown in [$C_4$mpy] [$NTf_2$] instead of others.

*Comparison of Methane oxidation at Au and Pt electrode in [$C_4$mpy] [$NTf_2$] and [$C_6$mpy] [$NTf_2$].*— Methane oxidation behavior was further characterized by CV at Au electrode in [$C_4$mpy] [$NTf_2$] and [$C_6$mpy] [$NTf_2$] ILs and the results were compared to those at Pt electrode. The positive potential applied at Pt electrode could activate the platinum electrode. We have performed an activation step for the Pt gauze electrodes used in our study. The Pt gauze electrode potential was scanned between 1.5 V to −1.8 V in which the Pt electrode could be activated at high potential.[43,44] As shown in Figure 5, there is no obvious anodic current increasing at 0.9 V related to methane oxidation on the gold electrode in both ILs. We found the methane oxidation and oxygen redox activity on the activated platinum are much higher than the non-activated Pt (i.e. without the initial potential scanning between 1.5 V to −1.8 V). However, we did not observe the difference when the same conditions were applied to the gold electrode. Even the peak current of oxygen reduction at Au electrode is 55% of that at activated Pt electrode in [$C_4$mpy] [$NTf_2$] supporting the Au electrode activity for reduction of oxygen is much lower than that at activated platinum electrode. At Au electrode, the CV shows S-shape curves of superoxide oxidation process, which was consistent with reports from Compton's group.[45] However on the activated platinum electrode, the electron transfer process is fast and the rate limiting process is by the mass transfer process, a peaked current -potential curve was found in oxygen reduction process. (Figure S4 and S5). Furthermore, the peak potential difference ($\Delta$Ep-$O_2$) between cathodic and anodic peak of oxygen redox process is larger on Au than that on the activated Pt electrode ($\Delta$Ep-$O_2$/Au > $\Delta$Ep-$O_2$/Pt). All these experiments results suggest different electron-transfer kinetics at Pt vs. Au in these two $NTf_2$ based ILs. The standard rate constant of certain reaction could be calculated from the Laviron equation,[46] in which

$$E_{pc} = E^{0'} - \frac{2.3RT}{\alpha nF} \log \upsilon \quad [1]$$

$$E_{pa} = E^{0'} + \frac{2.3RT}{(1-\alpha)nF} \log \upsilon \quad [2]$$

$$\log k = \alpha \log(1-\alpha) + (1-\alpha)\log\alpha - \log\frac{RT}{nF\upsilon} - \frac{(1-\alpha)\alpha F \Delta E_p}{2.3RT} \quad [3]$$

Here $\alpha$ is the electron-transfer coefficient, $k$ is the standard rate constant of reaction, $\upsilon$ is the scan rate, and $E^{0'}$ is the formal potential.

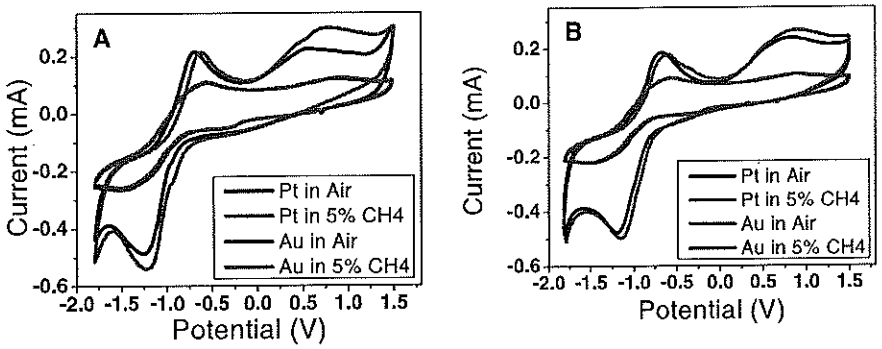


**Figure 5.** Cyclic voltammograms of Pt and Au electrode in (A) $[C_4mpy][NTf_2]$; (B) $[C_6mpy][NTf_2]$, with 100% dry air and 5% methane in air (500 mV $s^{-1}$ scan rate, 6th cycle).

The electrode activity was quantified for the oxygen reduction in the two $NTf_2$ based ILs (Table I).

In both ionic liquids, the standard rate constant of oxygen redox process on the activated platinum is more than 26 times higher than that on gold. Thus, activated platinum has much higher activity than gold for electrode reaction in the $NTf_2$ based ionic liquids.

Table II summarized our characterization of the methane oxidation on Pt, Au and carbon electrodes in four additional ILs with different anions and cations. At gold and carbon electrode, there is no oxidation of methane observed in all the ILs tested. ILs with anions other than $NTf_2$ shows little or no methane oxidation. The methane oxidation was observed at platinum electrode in $NTf_2$-based ILs only. The cations in $NTf_2$-based ILs also play significant roles with $[C_4mpy][NTf_2]$ showing the higher methane oxidation currents than that of $[C_6mpy][NTf_2]$.

*In-situ FTIR spectroelectrochemistry characterization of methane oxidation.*— In-situ FTIR spectroelectrochemistry was used to characterize the $[C_4mpy][NTf_2]$ and Pt interfaces during methane oxidation process. In-situ FTIR spectroelectrochemistry is especially beneficial for studying IL and Pt interface since the organic nature of ILs allows the monitoring of the products or intermediates of reaction on the electrode surface as a function of applied potential without the interference from water and solvents encountered in most aqueous or non-aqueous systems.

Figure 6 shows the in-situ reflectance FTIR spectra in $[C_4mpy][NTf_2]$ at Pt interface. From Figure 6A, the dark red curve is a typical FTIR spectrum of $[C_4mpy][NTf_2]$ on the Pt. With 5% methane purging into the system, the water peak at 3400 $cm^{-1}$ decreased, which was shown as orange curve in Figure 6A. The Henry's constant of methane in $[C_4mpy][NTf_2]$ is about 300 bar which is much smaller than that of nitrogen and oxygen at room temperature.[47,48] The adsorption of methane in $[C_4mpy][NTf_2]$ can be observed around 3000 $cm^{-1}$. According to IR surface selection rule, only the adsorbate modes with a dipole moment component perpendicular to the reflecting surface can interact with the IR beam. Strong multiple bands at 2989, 2872 and 1308 $cm^{-1}$ are observed in methane IR spectra. The 2989 $cm^{-1}$ band is assigned to the $\nu_3$ (antisymmetric) C–H stretching mode, which appears at 3020 $cm^{-1}$ in free $CH_4$.[49,50] The band around 2872 $cm^{-1}$ arises from the $\nu_1$ (symmetric stretch). The appearance of an infrared forbidden vibration mode $\nu_1$ is a strong indication of methane absorption. The band at 1308 $cm^{-1}$ is ascribed to the $\nu_4$ mode (deform) of the adsorbed methane.[51,52] Shown in Figures 4 and S4, the methane oxidation peak was around at 0.9 V. When the potential of 0.9 V was applied on the Pt working electrode for 60 minutes (green curve in Figure 6A and Figure 6B), these multiple peaks

**Table I. The standard rate constant ($k$) of oxygen redox reaction on Pt and Au electrodes in two ionic liquids.**

| $k$ ($s^{-1}$) | Pt | Au |
|---|---|---|
| $[C_4mpy]$ $[NTf_2]$ | 0.0509 | 0.0019 |
| $[C_6mpy]$ $[NTf_2]$ | 0.0417 | 0.0013 |

**Table II. The peak current at 0.9 V for methane oxidation on the different electrodes in ionic liquids with variable ionic components.**

| | Pt | Au | Carbon |
|---|---|---|---|
| $[C_4mpy][NTf_2]$ | $2.14 \times 10^{-5}$ A | N/A | N/A |
| $[C_6mpy][NTf_2]$ | $1.21 \times 10^{-5}$ A | N/A | N/A |
| $[C_4mim][NTf_2]$ | $<10^{-6}$ A | N/A | N/A |
| $[C_4mpy][FAP]$ | N/A | N/A | N/A |
| $[C_4mpy][PF_6]$ | N/A | N/A | N/A |
| $[C_4mpy][Beti]$ | N/A | N/A | N/A |

N/A means no obvious anodic current of methane.

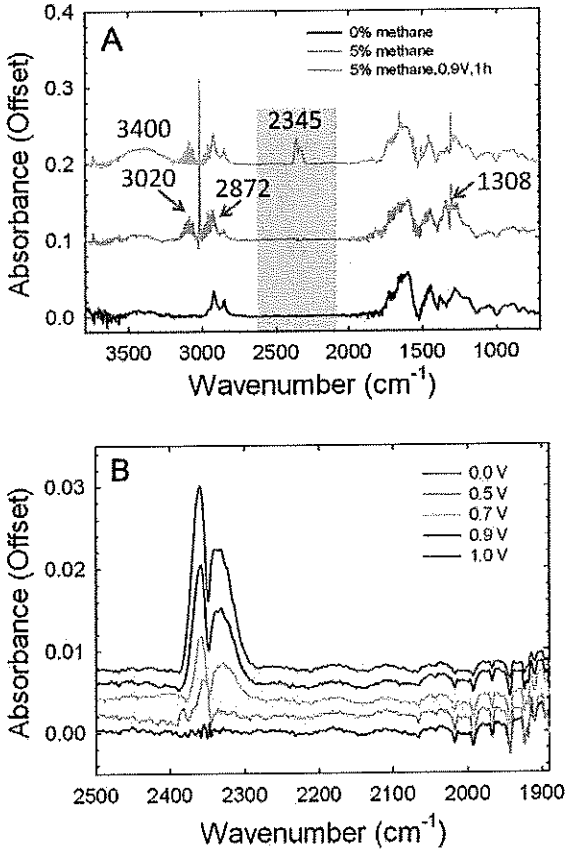


**Figure 6.** In-situ $p$-type polarized FTIR reflectance spectra of (A) $[C_4mpy][NTf_2]$ and Pt interface with zero methane (pure oxygen) or 5 vol.% methane (oxygen as diluting gas) without applied potential and after applying potential at 0.9 V for 60 mins. (B) Methane electro-oxidation by applying varying potentials (0.0, 0.5 V, 0.7 V, 0.9 V, 1.0 V) for 60 mins. 5 vol.% methane (oxygen as dilution gas).

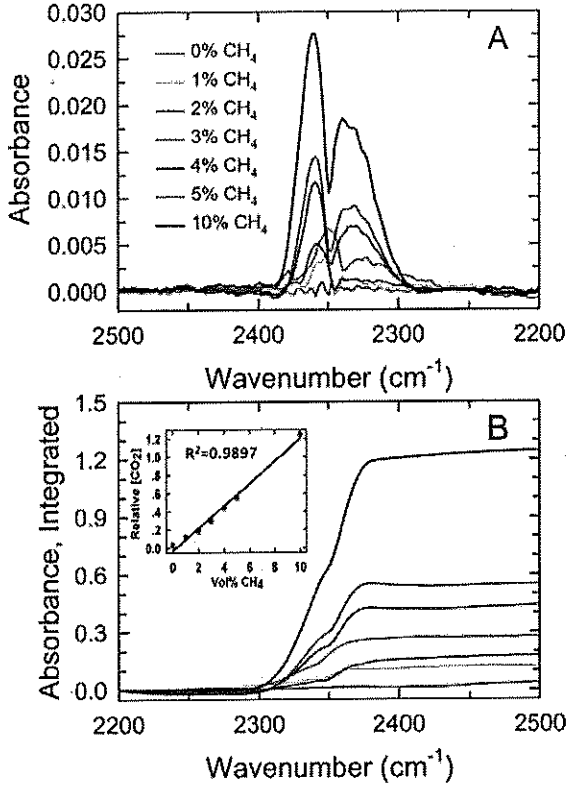


**Figure 7.** (A) FTIR spectra acquired during methane electro-oxidation at different methane concentrations (Oxygen as diluting gas) at 0.9 V. (B) Integrated absorbance of the $CO_2$ peak as a function of wavenumber at various methane concentrations. Inset: Normalized $CO_2$ concentration from FTIR results versus methane concentration.

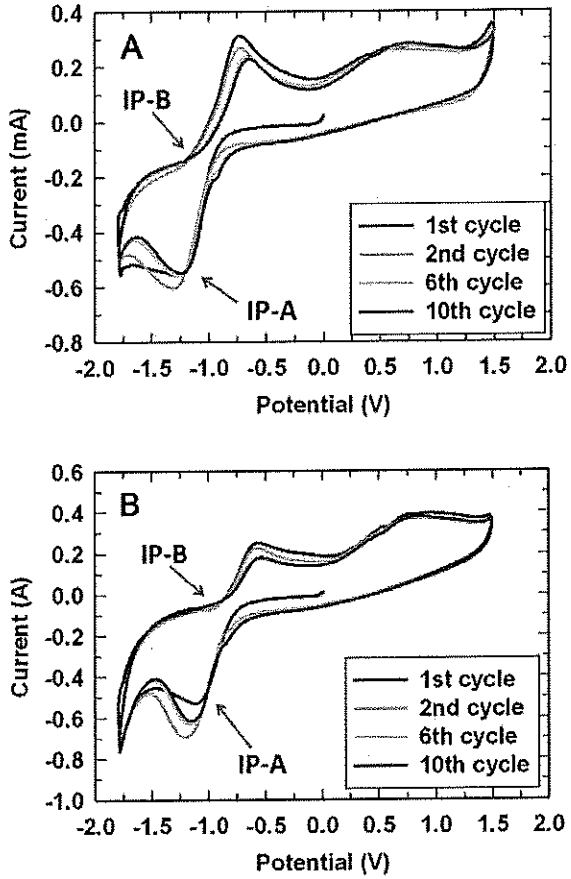


**Figure 8.** Cyclic voltammograms of 1st, 2nd, 6th and 10th cycle in (A)5% methane, (B) 25% methane in $[C_4mpy][NTf_2]$. Cycle 1–25 data is in supplementary file (500 mV $s^{-1}$ scan rate).

were reduced, compared with the results at open circuit in which no potential is applied to the electrode. Methane electro-oxidation at 0.9 V leads to the appearance of double peaks in IR which is consistent with a $CO_2$ peak at 2345 $cm^{-1}$ and a broad band peak at 3400 $cm^{-1}$ related to water.[53] It is noted that, different from experiments in aqueous solutions, there are no bands found around 2100 $cm^{-1}$. This observation suggests that the molecular species like CO, COOH and CHO, the incomplete products of oxidation of hydrocarbon such as methane observed in other systems are not observed in our studied system. The methane oxidation products in $[C_4mpy][NTf_2]$ were only $CO_2$ and $H_2O$, and $CO_2$ generated was dissolved into ionic liquid instead of adsorbing on the platinum electrode surface, since there is no $CO_2$ adsorption peak (2038 $cm^{-1}$) emerged.[54] $CO_2$ has high solubility in ionic liquids which minimize the possibility of the $CO_2$ adsorption at the Pt active sites. The results of the in-situ FTIR spectroelectrochemistry study with different methane concentrations at 0.9 V are shown in Figure 7. With increasing of the concentration of methane, the $CO_2$ peak around 2345 $cm^{-1}$ increased. The peak area, which was related to $CO_2$ concentration, was integrated and plotted against methane concentration. A linear relationship was obtained with methane concentration as shown in inset graph in Figure 7B.

FITR results confirmed that the products of methane electro-oxidation in $[C_4mpy][NTf_2]$ are $H_2O$ and $CO_2$ with no other detectable incomplete oxidation species presented during the whole oxidation process. This result has high significance for using methane in energy conversion and sensor development since CO and other incomplete oxidation products of methane were reported to poison Pt electrode. There is also no obvious peak shifts related to the $[C_4mpy][NTf_2]$, which implies that during the methane oxidation, IL structure at interface remains intact.

*Cyclic voltammetry characterization of methane oxidation in $[C_4mpy][NTf_2]$ and the coupling reaction with superoxide due to oxygen reduction.*— The CV curves in Figure 3 and Figure 5 also show that in the presence of methane and in both $NTf_2$ based ILs, peak potentials of oxygen reduction and superoxide oxidation processes shifted to more positive direction and the peak currents of oxygen reduction increases and the peak current of superoxide oxidation decreases. These phenomena are strong indications of EC mechanism, i.e. an electrode reaction coupled with a chemical reaction[39,55–58] due to the presence of water and $CO_2$ on the electrode as the products of methane oxidation. We further characterize the redox processes of oxygen and methane in $[C_4mpy][NTf_2]$/Pt in detail by multiple cycle CVs. Figure 8 shows the CV curves of multiple cycles in 5% and 25% methane conditions. In these experiments, in the first cycle, the potential was conditioned at 0.0 V and scanned to the negative potential −1.8 V. Then the potential was subsequently scanned between −1.8 V to 1.5 V (all cycles of CV curves are shown in figure S6 and S7). There are several important observations of these CV results that further support our interpretation of the methane oxidation process. (1) At methane oxidation region (more positive than 0.6 V), the anodic current remains constant during the multiple-potential cycling. This suggests there is no electrode poisoning by the incomplete methane oxidation products as reported in many other methane catalytical systems in which the following sweep in the cyclic voltammetry attests to the strong deactivation of platinum electrode by the decrease of the anodic current[59–62] due to the adsorbed organic residues and CO derived from the oxidation of methane in other systems during the sustained oxidation.[63–67] The backflow electrochemical cell design used in this work facilitates the quick removal of the products at the

electrode/electrolyte interface; (2) In the first cathodic scan, a cathodic peak at −1.1 V is observed. This is due to the oxygen reduction to form superoxide radical which was being re-oxidized at −0.7 V at the subsequent anodic scan. A broad anodic peak at 0.5 V is due to the oxidation of Pt,[68] since it is not appeared in nitrogen condition (Figure S5). In the presence of methane, the peak located around 0.9 V is attributed to methane oxidation, which was not found in absence of methane condition; (3) In the second and subsequent cathodic scan cycles, a new small cathodic peak was observed at −0.8 V. This new cathodic peak was attributed to the oxygen reduction in the presence of $H_2O$ on the electrode.[17,69] But this peak is relative small since the amount of $H_2O$ generated here is limited. This peak only exists in the third scan cycle when methane is at 5 vol% but it emerges at the second scan cycle in 25 vol% methane since the higher concentration methane could generate more $H_2O$ as products. Further supporting this rationalization is the observation of increasing peak current of the oxygen reduction peak at −1.1 V and the decreasing of the superoxide oxidation peak in the second cycle and subsequent cycles. As a comprehensive review of superoxide ion chemistry given by Sawyer et al.,[70] the superoxide ion can be formed electrochemically via direct cathodic reduction of oxygen. It is a strong nucleophile which disproportionates with $CO_2$ to $O_2$. AlNashef et. al[55,71] reported this phenomenon in ILs as well that the increase in the oxygen reduction current and the decrease of superoxide oxidation current is the characteristic of a reaction in which $O_2$ is regenerated to produce the net effect of an irreversible two-electron reduction of $O_2$ at the presence of $CO_2$. Even though the methane concentration was maintained by a constant gas flow, as the methane oxidation product, $H_2O$ and $CO_2$ could not be removed instantly since scan time is short and viscosity of ionic liquid is high. During the continuous potential scanning, more of $CO_2$ and $H_2O$ were produced and accumulated on the Pt working electrode surface. It could occupy the electrode active sites that results in the decrease of subsequent oxygen reduction current compared with the second cycle. In both 5% and 25% methane systems, from the 6th potential scanning cycle, the following CV curves of methane and oxygen redox processes are overlapped. We believe that after six cycle potential scanning a gas feed-remove balance has been established, in which the species on the electrode reach to a steady state. The magnitudes of the change of peak current and peak positions of oxygen redox processes at various methane concentrations and scan cycles were the results of these effects as well; (4) The observation of the isopotential points (IP) in these multiple potential cycling experiments substantiates the surface processes occurred in the methane oxidation processes at the Pt electrode. As defined by Bruckenstein et. al,[72,73] an isopotential point occurs at an electrode surface which is partially covered with at least one adsorbed or deposited species at the start of the application of the potential program, the initial amount of adsorbed or deposited species is different for each curve, and the electrode surface behaves as if it consists of two independent electrochemical regions and the sum of those areas is constant at all times for all of the current –potential curves. Two isopotential points (IP-A and IP-B in Figure 8A and 8B were observed for curves 1–10th respectively in cathodic and anodic scan in the oxygen reduction and superoxide oxidation potential window. Since these isopotential points lie on the residual I-E curve, the oxidation of methane and/or Pt must be one of the processes giving rise to these points. We believe that IP-A and IP-B involved the reduction of $O_2$ in the presence of methane oxidation product of $H_2O$ and $CO_2$. Our explanation for IP-A and IP-B is that the oxygen has been adsorbed at electrode region of area ($A_{Oxygen}$) while on the reminder of the electrode, area $A_{Methane}$ is the adsorbed methane. On the anodic sweep, at area of $A_{Methane}$, the simultaneous oxidation of adsorbed methane and Pt at current density $i_{Methane}$ will generated $CO_2$ and $H_2O$ adsorbed which participated in the oxygen reduction processed at the electrochemically independent region of area $A_{Oxygen}$ at current density $i_{Oxygen}$. When the current density for all processes on one of the regions equals the current density for all processes on the other regions, the isopotential points occur; (5) The peaks of PtOx around 0.5 V were observed before methane oxidation peak at around 0.9 V. The shoulder peak of oxygen reduction at −0.8 V appeared only after the second cycle indicating it's related to the water and $CO_2$ produced by methane oxidation. It suggests that methane prefers to adsorb on the PtOx surface or Pt-Ox surface; (6) From Figure 8A, the methane anodic current increased a little bit during the potential scanning. It may be due to the trace amount of water produced from methane oxidation since it was reported that the oxidation of organic species by surface oxides on Pt are facilitated by the oxidation of water over Pt to form Pt-OH ($H_2O + Pt \rightarrow Pt\text{-}OH + H^+ + e^-$) under positive potential.[74,75]

*Mechanisms of methane oxidation in $NTf_2$ based ILs.*— The mechanisms of electro-oxidation of methane were studied in the acidic aqueous electrolytes and proposed as an eight electron process by Bockris et al. in 1965.[76] The adsorption process proceeds via physisorption of methane on the platinum surface followed by dissociation of the adsorbed methane molecule to an adsorbed methyl group and adsorbed hydrogen which is oxidized immediately, as expressed by eq 4.

$$CH_4 + 2H_2O \rightarrow CO_2 + 8H^+ + 8e^- \quad [4]$$

In aqueous solution, $CH_4$ has to dissociate at the electrode surface to be $CH_x$ ($x = 0$–3) species which can then be converted to CO through a series of surface reactions. Typically, strong acids were employed as oxidants, however, the protonation from acids could limit further dissociation of methane and cause incomplete oxidation (the product would be CO).[77] Our above results suggest that methane oxidation follows a different pathway compared with those proposed in the acidic aqueous solution. Since only in $NTf_2$ based ILs that methane could be oxidized at Pt electrode. It means $NTf_2$ plays a significant role in methane oxidation. We believe $NTf_2$ anion contributes to the methane oxidation process. Comparing the nucleophilicity of $[NTf_2]^-$ with $[O_2]^-$ in the IL, the latter has a higher activity for the metal and is therefore more strongly bound to the metal electrode surface. Our experiments show that the initial oxidation of Pt surface is a significant process that determines the reactivity of electrocatalytical oxidation of methane which is consistent with the simulation study of methane oxidation at Pt by Zhdanov, V. P. et.al.[68] Their study suggests that methane oxidation occurs in two step kinetics with a low reactive state with the surface completely covered by platinum oxide and a high-reactive state with the surface covered by the chemisorbed oxygen. Thus, we rationalize that at Pt electrode, Pt-O is the predominantly active site where methane oxidation takes place on this Pt oxide layer. The ILs can provide a strong polar environment, wherein the C–H bond in methane can be activated electrostatically. Once H dissociated from $CH_4$, further polarization of CHx makes it even easier to dissociate additional C–H bonds. Based on above evidence and rationalization, we propose the following methane oxidation mechanism in $NTf_2$ based ILs. In step 1, oxygen molecule was supplied from the gas phase via irreversible dissociative adsorption on Pt vacant sites

$$2Pt + O_2 \rightleftharpoons 2\,Pt\text{-}O(ads) \quad [5]$$

where Pt-O is the adsorption form of oxygen in the surface layer. Oxygen atom can diffuse in and between the Pt atomic layers resulting Pt surface reconstruction. Under the positive potential, it is easy to form the Pt oxide on the electrode surface. In $NTf_2$-based ionic liquid system, $NTf_2^-$ could adsorb on the metallic oxide surface adapting the structure of the metal surface.[21] $NTf_2^-$ typically behaves as a weak or non-coordinating anion.[78] However, a weak Pt-$NTf_2$ coordinate complex likely occurs in the absence of other ligands.[79,80] The formation of Pt-$NTf_2$ adsorbate shown in eq. 5 which could have high catalytic activity:

$$Pt\text{-}O + NTf_2^- \rightleftharpoons O\text{-}Pt\text{-}NTf_2^- \rightleftharpoons O\text{-}Pt\text{-}NTf_2^{\bullet} + e \quad [6]$$

As reported, Pt (II) centered complex has strong coordination with C-H bond, which was reported for activation methane in organic chemistry.[3,4,81] Here we in-situ generated O-Pt-$NTf_2^{\bullet}$ electrochemically which could have very high activity of binding with other atoms such as methane than Pt oxide.[82,83] The reaction is considered to be limited by the dissociative chemisorptions of $CH_4$ occurring via the

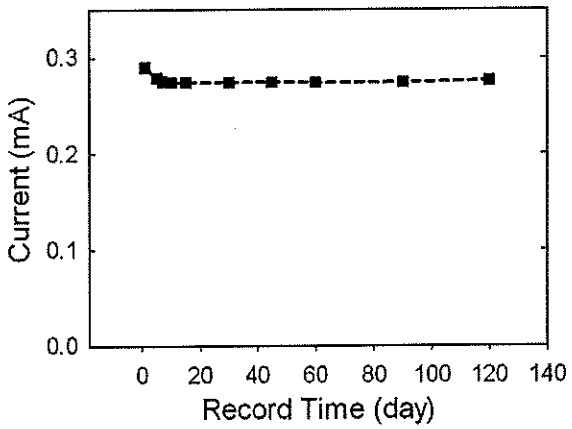


**Figure 9.** Methane oxidation current at $[C_4mpy][NTf_2]$/Pt interface under 200 sccm continuous 5 vol.% methane in dry air flow. Peak current of 0.9 V were measured during CV experiment (500 mV/s).

Eley-Rideal-type mechanism by breaking of C–H bonds.[84,85] Usually the free radical could exist in a condensed medium and ILs can be considered as a condensed medium due to the high viscosity and the big size of the ion limiting its ion mobility.

$$4\,\text{O-Pt-NTf}_2^{\bullet} + CH_4 \rightleftharpoons CO_2 + 2\,H_2O + 4\,\text{Pt-NTf}_2^{\bullet} \quad [7]$$

Here $H_2O$ generated from methane could adsorb on the Pt electrode surface since $[C_4mpy][NTf_2]$ is hydrophobic, and it could react with Pt via following processes to form Pt-OH.[74,75]

$$H_2O + \text{surface free site}^{*} \rightleftharpoons OH_{ads} + H^{+} + e \quad [8]$$

and

$$Pt + H_2O \longrightarrow \text{Pt-OH} + H^{+} + e \quad [9]$$

Since surface bonded OH is the oxygen donor reacting with surface bonded CO to form $CO_2$. It is likely that Pt-OH could form in our system in the presence of methane facilitating methane oxidation to $CO_2$.[74,75] There is no band related to CO found in FTIR spectrum during the methane oxidation. We propose that the total reaction is

$$CH_4 + O_2 \xrightarrow{\text{Pt/NTf}_2\text{-IL}} CO_2 + 2H_2O \quad [10]$$

Taking into account that methane oxidation process in non-aqueous electrolyte was a four electron process, the oxidized Pt electrode reactivity is also dependent on the adsorption of $[C_4mpy][NTf_2]$. $[C_4mpy][NTf_2]$ not only was employed as a solvent and supporting electrolyte, but also adsorption on the $[C_4mpy][NTf_2]$ –Pt interface affects the surface catalytic activity of platinum oxide by solvating the reactive species, although we are not able to observe oxygen signal and changes of $[C_4mpy][NTf_2]$ peaks in IR spectrum due to lack of sensitivity of FTIR to measure the catalytic intermediates at electrode IL interface.

*Long-term stability of methane oxidation in IL.*— the methane oxidation products $CO_2$ and $H_2O$ can be easily removed from the electrode –IL interface by carrier gas flow. This maintains a constant $[C_4mpy][NTf_2]$/Pt interface and should lead to a stable anodic current of methane oxidation for long-term applications. Figure 9 shows the peak current at 0.9 V vs. time curve obtained in CV measurements with 5 vol.% methane in dry air condition tested during 4 months period. Between testing, the Pt and $[C_4mpy]$ $[NTf_2]$ electrode was exposed to $N_2$. The current of $[C_4mpy][NTf_2]$/Pt system only showed 5% variable over the first week, and remained almost constant during the remaining time of the experiment proving that $[C_4mpy]$ $[NTf_2]$ /Pt electrode interface for methane oxidation is very stable compared with current catalyst electrochemical systems. Thus, $[C_4mpy]$ $[NTf_2]$ /Pt system will be very promising for applications in sensors and fuel cells with long-term stable power output and reliable sensor measurements.

## Conclusions

We have systematically characterized the methane oxidation process in several ILs at Pt, Au and carbon electrodes under aerobic conditions. Our results confirms that methane could be fully oxidized only at $NTf_2$ based ILs ($[C_6mpy][NTf_2]$ and $[C_4mpy][NTf_2]$) at Pt electrode in room temperature. Our results suggest that the methane oxidation depends not only on oxygen concentration and Pt electrode potential but also is governed by the properties of IL. The more compact double layer associated with $[C_4mim][NTf_2]$ prevents methane oxidation whereas the more loosely-packed double layer formed in $[C_4mpy][NTf_2]$ allows for facile methane oxidation. The methane oxidation in $[C_4mpy][NTf_2]$ and Pt under air/oxygen was thoroughly characterized by CV and spectroelectrochemistry (in-situ FTIR) techniques. The product of methane oxidation is water and $CO_2$ confirmed by the CV and in-situ IR spectroelectrochemistry results. We proposed a multiple step mechanism involving methane adsorption and platinum oxide formation in which at least a portion of a surface of a platinum working electrode is activated at an interface between the platinum working electrode and an ionic liquid electrolyte (i.e., 1-ethyl-1-methylpyrrolidinium bis(trifluoromethylsulfonyl)imide). An interface complex O-Pt-$NTf_2$ · is likely formed at the electrode and ionic liquid interface and methane adsorbs at or near this interface complex. Our proposed mechanism has not been observed in early studies of hydrocarbon electro-oxidation,[8,29,86–88] but can fully explain our observed results. Due to absence of incomplete oxidation products of CO, the IL and Pt interface maintains the activity for a long time. There was only 0.5% of current drift in 120 days under air condition. The findings of this work prove useful to improve operating conditions and selectivity leading to practical methane sensors using ILs that is simultaneously robust, sensitive, stable, and selective. The understanding of methane oxidation process in ILs also opens up new opportunities in electrocatalysis of methane which can enable the use of methane as an electrochemical energy storage material for portable power applications and long-term stable power supply device. The beneficial features of IL electrochemical systems can be extended for applications in electrochemical oxidations of other hydrocarbons as well.

*Electronic supplementary information (ESI) available.*— Figure S1-S7 and table S1 are provided as supplementary information.

## Acknowledgment

X. Z. thank NIOSH R21 (Grant No. R21OH009099) for financial support of this work. Dr. Chaminda Hettige proofread this paper, Min Guo did additional experiments. We thank Dr. Mike Sevilla for helpful discussions.

## References

1. R. H. Crabtree, *Chem Rev*, **95**(4), 987 (1995).
2. E. E. Wolf, *Methane conversion by oxidative processes: fundamental and engineering aspects*, Van Nostrand Reinhold, New York (1992).
3. G. S. Chen, J. A. Labinger, and J. E. Bercaw, *Proceedings of the National Academy of Sciences*, **104**(17), 6915 (2007).
4. A. E. Shilov and G. B. Shul'pin, *Chem Rev*, **97**(8), 2879 (1997).
5. R. A. Periana, D. J. Taube, S. Gamble, H. Taube, T. Satoh, and H. Fujii, *Science*, **280**(5363), 560 (1998).
6. D. A. Hickman and L. D. Schmidt, *Science*, **259**(5093), 343 (1993).
7. S. Scheller, M. Goenrich, R. Boecher, R. K. Thauer, and B. Jaun, *Nature*, **465**(7298), 606 (2010).
8. T. Otagawa, S. Zaromb, and J. R. Stetter, *J. Electrochem Soc*, **132**(12), 2951 (1985).
9. T. Hibino, A. Masegi, and H. Iwahara, *J. Electrochem Soc*, **142**(5), L72 (1995).
10. V. Roche, R. Revel, and P. Vernoux, *Catal Commun*, **11**(13), 1076 (2010).
11. M. M. Slinko, *Catal Today*, **154**(1–2), 38 (2010).
12. M. Stoukides, *J Appl Electrochem*, **25**(10), 899 (1995).
13. B. G. Hashiguchi, S. M. Bischof, M. M. Konnick, and R. A. Periana, *Accounts Chem Res*, **45**(6), 885 (2012).
14. R. J. Soukup-Hein, M. M. Warnke, and D. W. Armstrong, *Annu. Rev. Anal. Chem.*, **2** 145 (2009).
15. G. A. Baker, S. N. Baker, S. Pandey, and F. V. Bright, *Analyst*, **130**(6), 800 (2005).

16. W. Lu, A. G. Fadeev, B. H. Qi, E. Smela, B. R. Mattes, J. Ding, G. M. Spinks, J. Mazurkiewicz, D. Z. Zhou, G. G. Wallace, D. R. MacFarlane, S. A. Forsyth, and M. Forsyth, *Science*, **297**(5583), 983 (2002).
17. Z. Wang, P. Lin, G. A. Baker, J. Stetter, and X. Zeng, *Anal Chem*, **83**(18), 7066 (2011).
18. J. P. Hallett and T. Welton, *Chem Rev*, **111**(5), 3508 (2011).
19. P. Hapiot and C. Lagrost, *Chem Rev*, **108**(7), 2238 (2008).
20. S. Baldelli, *Accounts Chem Res*, **41**(3), 421 (2008).
21. M. Sobota, I. Nikiforidis, W. Hieringer, N. Paape, M. Happel, H. P. Steinruck, A. Gorling, P. Wasserscheid, M. Laurin, and J. Libuda, *Langmuir*, **26**(10), 7199 (2010).
22. D. B. Williams, M. E. Stoll, B. L. Scott, D. A. Costa, and W. J. Oldham, *Chem Commun*, 11, 1438 (2005).
23. F. Duris, D. Barbier-Baudry, A. Dormond, J. R. Desmurs, and J. M. Bernard, *J Mol Catal a-Chem*, **188**(1–2), 97 (2002).
24. J. P. Hallett and T. Welton, *Chem Rev*, **111**(5), 3508 (2011).
25. T. Welton, *Chem Rev*, **99**(8), 2071 (1999).
26. P. Kilaru, G. A. Baker, and P. Scovazzo, *J. Chem. Eng. Data*, **52**(6), 2306 (2007).
27. A. K. Burrell, R. E. D. Sesto, S. N. Baker, T. M. McCleskey, and G. A. Baker, *Green Chem.*, **9**(5), 449 (2007).
28. S. N. Baker, T. M. McCleskey, S. Pandey, and G. A. Baker, *Chem Commun*, 8, 940 (2004).
29. T. Otagawa, S. Zaromb, and J. R. Stetter, *Sensors and Actuators*, **8**(1), 65 (1985).
30. P. Hrncirova and F. Opekar, *Sensor Actuat B-Chem*, **81**(2–3), 329 (2002).
31. F. Opekar and K. Stulik, *Anal Chim Acta*, **385**(1–3), 151 (1999).
32. C. H. Xiao, A. Rehman, and X. Q. Zeng, *Anal Chem*, **84**(3), 1416 (2012).
33. L. Cammarata, S. G. Kazarian, P. A. Salter, and T. Welton, *Phys Chem Chem Phys*, **3**(23), 5192 (2001).
34. F. Endres and S. Z. El Abedin, *Phys Chem Chem Phys*, **8**(18), 2101 (2006).
35. H. Munakata, T. Tashita, M. Haibara, and K. Kanamura, *ECS Transactions*, **33**(7), 463 (2010).
36. A. Rehman, A. Hamilton, A. Chung, G. A. Baker, Z. Wang, and X. Q. Zeng, *Anal Chem*, **83**(20), 7823 (2011).
37. R. Ojani, J. B. Raoof, and B. Norouzi, *J Solid State Electr*, **15**(6), 1139 (2011).
38. M. A. Xu, B. R. Bunes, and L. Zang, *ACS Appl. Mater. Interfaces*, **3**(3), 642 (2011).
39. M. C. Buzzeo, O. V. Klymenko, J. D. Wadhawan, C. Hardacre, K. R. Seddon, and R. G. Compton, *J. Phys. Chem. A*, **107**(42), 8872 (2003).
40. O. Deutschmann, L. I. Maier, U. Riedel, A. H. Stroemman, and R. W. Dibble, *Catal Today*, **59**(1–2), 141 (2000).
41. A. H. Taylor and S. B. Brummer, *J Phys Chem-Us*, **72**(8), 2856 (1968).
42. Z. Wang, X. Mu, M. Guo, Y. Huang, A. J. Mason, and X. Zeng, *J Electrochem Soc*, **160**(6), B83 (2013).
43. W. C. Barrette and D. T. Sawyer, *Anal Chem*, **56**(4), 653 (1984).
44. D. S. Silvester, L. Aldous, C. Hardacre, and R. G. Compton, *J Phys Chem B*, **111**(18), 5000 (2007).
45. A. S. Barnes, E. I. Rogers, I. Streeter, L. Aldous, C. Hardacre, G. G. Wildgoose, and R. G. Compton, *J Phys Chem C*, **112**(35), 13709 (2008).
46. E. Laviron, *J Electroanal Chem*, **101**(1), 19 (1979).
47. R. D. Noble, A. Finotello, J. E. Bara, and D. Camper, *Ind Eng Chem Res*, **47**(10), 3453 (2008).
48. J. F. Brennecke, J. L. Anderson, and J. K. Dixon, *Accounts Chem Res*, **40**(11), 1208 (2007).
49. A. M. Ferrari, S. Huber, H. Knozinger, K. M. Neyman, and N. Rosch, *J Phys Chem B*, **102**(23), 4548 (1998).
50. S. Huber and H. Knozinger, *Chem Phys Lett*, **244**(1–2), 111 (1995).
51. D. Scarano, S. Bertarione, G. Spoto, A. Zecchina, and C. O. Arean, *Thin Solid Films*, **400**(1-2), 50 (2001).
52. C. Li, W. H. Yan, and Q. Xin, *Catal Lett*, **24**(3–4), 249 (1994).
53. C. Zhao, A. M. Bond, R. G. Compton, A. M. O'Mahony, and E. I. Rogers, *Anal Chem*, **82**(9), 3856 (2010).
54. B. Westerhoff and R. Holze, *Ber Bunsen Phys Chem*, **97**(3), 418 (1993).
55. I. M. AlNashef, M. L. Leonard, M. C. Kittle, M. A. Matthews, and J. W. Weidner, *Electrochem Solid St*, **4**(11), D16 (2001).
56. I. M. AlNashef, M. L. Leonard, M. A. Matthews, and J. W. Weidner, *Ind Eng Chem Res*, **41**(18), 4475 (2002).
57. M. C. Buzzeo, E. V. Klymenko, J. D. Wadhawan, C. Hardacre, K. R. Seddon, and R. G. Compton, *J Phys Chem B*, **108**(12), 3947 (2004).
58. V. Y. Antonchenko and E. S. Kryachko, *Chem Phys*, **327**(2–3), 485 (2006).
59. K. Jambunathan, B. C. Shah, J. L. Hudson, and A. C. Hillier, *J Electroanal Chem*, **500**(1–2), 279 (2001).
60. S. Park, R. Craciun, J. M. Vohs, and R. J. Gorte, *J Electrochem Soc*, **146**(10), 3603 (1999).
61. K. Sato, J. Nakamura, T. Uchijima, T. Hayakawa, S. Hamakawa, T. Tsunoda, and K. Takehira, *J Chem Soc Faraday T*, **91**(11), 1655 (1995).
62. B. C. Shah and A. C. Hillier, *J. Electrochem Soc*, **147**(8), 3043 (2000).
63. I. Bar-Nahum, A. M. Khenkin, and R. Neumann, *J Am Chem Soc*, **126**(33), 10236 (2004).
64. R. J. Gorte, S. Park, J. M. Vohs, and C. H. Wang, *Adv Mater*, **12**(19), 1465 (2000).
65. H. Hoster, T. Iwasita, H. Baumgartner, and W. Vielstich, *J. Electrochem Soc*, **148**(5), A496 (2001).
66. E. Herrero, K. Franaszczuk, and A. Wieckowski, *J Phys Chem-Us*, **98**(19), 5074 (1994).
67. S. M. Park, N. C. Chen, and N. Doddapaneni, *J Electrochem Soc*, **142**(1), 40 (1995).
68. V. P. Zhdanov, P. A. Carlsson, and B. Kasemo, *J Chem Phys*, **126**(23), 234705 (2007).
69. Z. Wang, M. Guo, G. A. Baker, J. Stetter, and X. Zeng, (in review).
70. D. T. Sawyer and J. L. Roberts, *J. Electroanal. Chem.*, **12**, 90 (1966).
71. M. V. Merritt and D. T. Sawyer, *The Journal of Organic Chemistry*, **35**(7), 2157 (1970).
72. D. F. Untereker and S. Bruckenstein, *Anal Chem*, **44** (6), 1009 (1972).
73. S. H. Cadle and S. Bruckenstein, *Anal Chem*, **44**(12), 1993 (1972).
74. M. T. M. Koper, S. C. S. Lai, and E. Herrero, in *Fuel Cell Catalysis*, p. 159, John Wiley & Sons, Inc., (2008).
75. M. Watanabe and H. Uchida, in *Fuel Cell Catalysis*, p. 317, John Wiley & Sons, Inc., (2008).
76. J. O. M. Bockris, E. Gileadi, and G. E. Stoner, *J. Phys. Chem.*, **73**(2), 427 (1969).
77. M. G. Sustersic, R. Cordova, W. E. Triaca, and A. J. Arvia, *J Electrochem Soc*, **127**(6), 1242 (1980).
78. B. Mathieu and L. Ghosez, *Tetrahedron*, **58**(41), 8219 (2002).
79. D. J. Liston, Y. J. Lee, W. R. Scheidt, and C. A. Reed, *J Am Chem Soc*, **111**(17), 6643 (1989).
80. J. Foropoulos and D. D. Desmarteau, *Inorg Chem*, **23**(23), 3720 (1984).
81. J. M. Villalobos, A. J. Hickman, and M. S. Sanford, *Organometallics*, **29**(1), 257 (2010).
82. R. A. Himes and K. D. Karlin, *P Natl Acad Sci USA*, **106**(45), 18877 (2009).
83. V. P. Zhdanov, P. A. Carlsson, and B. Kasemo, *J Chem Phys*, **126** (23), 234705 (2007).
84. V. P. Zhdanov and B. Kasemo, *J. Catal*, **195**(1), 46 (2000).
85. R. Burch and T. C. Watling, *J. Catal*, **169**(1), 45 (1997).
86. D. H. Geske, *J Am Chem Soc*, **81**(16), 4145 (1959).
87. P. L. Fabre, J. Devynck, and B. Tremillon, *Tetrahedron*, **38**(17), 2697 (1982).
88. D. B. Clark, M. Fleischmann, and D. Pletcher, *J Electroanal Chem*, **42**(1), 133 (1973).